Todo list

OBSERVATIONS OF PWNE WITH THE FERMI GAMMA-RAY SPACE TELESCOPE

A DISSERTATION
SUBMITTED TO THE DEPARTMENT OF PHYSICS
AND THE COMMITTEE ON GRADUATE STUDIES
OF STANFORD UNIVERSITY
IN PARTIAL FULFILLMENT OF THE REQUIREMENTS
FOR THE DEGREE OF
DOCTOR OF PHILOSOPHY

Joshua Jeremy Lande
February 2013

I certify that I have read this dissertation and that, in my opinion, it is fully adequate in scope and quality as a dissertation for the degree of Doctor of Philosophy.

(Stefan Funk) Principal Adviser

I certify that I have read this dissertation and that, in my opinion, it is fully adequate in scope and quality as a dissertation for the degree of Doctor of Philosophy.

(Elliott Bloom)

I certify that I have read this dissertation and that, in my opinion, it is fully adequate in scope and quality as a dissertation for the degree of Doctor of Philosophy.

(Roger Romani)

Approved for the University Committee on Graduate Studies

Abstract

Two things fill the mind with ever-increasing wonder and awe, the more often and the more intensely the mind of thought is drawn to them: the starry heavens above me and the moral law within me." – Immanuel Kant

The launch of the *Fermi* Gamma-ray space telescope in 2008 offered an unprecedented view into the γ-ray sky.

All the things we can learn with the the Large Area Telescope (LAT)

Development of a new analysis method for studying spatially-extended PWNs using `pointlike`.

A monte-carlo validation of the analysis method.

Search for new spatially-extended sources with the LAT.

Observations of PWNs in the off-peak region of LAT detected pulsars.

Search for PWNs counterparts to TeV sources.

Using the population of PWNs to understand the radiation mechanism of PWNs.

Acknowledgement

Acknowkege the educational institutes which taught me physics: My high school HB Woodlawn, my undergraduate institution Marlboro College, and my Stanford University.

First, I would like to acknowlege those mentors who inspired me to get a PhD.

- Mark Dodge, my high school physics teacher.
- Ron Turner, my internship adviser at Analytic Services (ANSER) during the GWU Science and Engineering Apprentice Program (SEAP)
- Anthony Tyson at UC Davis for my SULI Internship
- Apurva Mehta and Sam Webb sam Web at SLAC SULI Internship.

During my PhD I was helped by an almost overwhelminlgy large number of people in the LAT collaboration.

People at Stanford/SLAC: Stefan Funk, Elliott Bloom, Markus Ackermann, Tobias Jogler, Junichiro Katsuta, Yasunobu Uchiyama, Seth Digel, James Chiang

`pointlike` collaborators: Matthew Kerr, Toby Burnett, Eric Wallace, Marshall Roth

Pulsar Collaborators: David Smith, Matthew Kerr, Peter den Hartog, Tyrel Johnson, Damien Parent, Ozlem Celik

Careful review of text: Jean Ballet, Johann Cohen-Tanugi

I would like to thank the PWNs people Thank the people in Bordeaux: Marianne Lemoine-Goumard, Romain Rousseau, and Marie-Hélène Grondin

Fermi SLAC Grad Students: Keith Bechtol, Alex Drlica-Wagner, Alice Allafort, Herman Lee Yvonne Edmonds, Bijan Berenji, Ping Wang, Warit Mitthumsiri

Joanne Bogart, Heather Kelly, Richard Dubois, Renata Dart, Stuart Marshall, and Glenn Morris for putting up with my computer problems.

Martha Siegel, Chris Hall, Ziba Mahdavi, awesome SLAC administrators. Maria Frank, Elva Carbajal, and Violet Catindig , awesome Stanford administrators.

Additional Astro Stanford Graduate Students: Helen Craig, Michael Shaw, Adam Van Etten, Kyle Watters

Additonal Graduate Students at Stanford: Dan Riley, Joel Frederico, Ahmed Ismail, Joshua Cogan, Kunal Sahasrabuddhe,

Contents

List of Tables

List of Figures

List of Acronyms

2CG the second COS-B catalog. 9

2FGL the second *Fermi* catalog. 20, 35

2PC the second *Fermi* pulsar catalog. 20

3EG the Third EGRET Catalog. 11

ACD Anti-Coincidence Detector. vii, 12

arcsec second of arc. 29

BPL broken-power law. 37

CGRO the Compton Gamma Ray Observatory. 10

CGS the Centimetre-Gram-Second System of Units. 37, 38

ECPL exponentially-cutoff power law. 37, 38

EGRET the Energetic Gamma Ray Experiment Telescope. xi, 9–11

ESA the European Space Agency. 9

FWHM full width at half maximum. 8

GBM Gamma-ray Burst Monitor. vii, 12

IC inverse Compoton. 6, 18, 28, 29, 32

LAT the Large Area Telescope. iv, v, vii–ix, 12, 19, 20, 45, 49

MIT the Massachusetts Institute of Technology. 6, 13

MSP millisecond pulsar. 24

NASA the National Aeronautics and Space Administration. 9, 10

NRL the Naval Research Laboratory. 13

NS neutron star. 13, 22, 23, 27

OSO-3 the Third Orbiting Solar Observatory. xi, 8, 9, 19

PL power law. 37, 38

PWN pulsar wind nebula. iv, v, ix, xii, 1, 6, 14, 22, 26, 28–32, 49

SA solid angle. 39, 40

SAS-2 the second Small Astronomy Satellite. 9, 10

SNR supernova remnant. 26, 29, 38

Chapter 1

Overview

In Chapter 2, we discuss the history of γ-ray astrophysics, ...

Chapter 2

Gamma-ray Astrophysics

2.1 Astronomy and the Atmosphere

Humans surely have, since the very beginning, stared into space and contemplated its brilliance. Stone circles in the Nabta Playa in Egypt are likely the first observed astronomical observatory and are believed to have acted as a prehistoric calendar. Dating back to the 5th century BC, they are 1,000 years older than stonehenge (McK Mahille et al. 2007).

Astronomy has historically been almost entirely concerned with studying the photons that arrive from outer space. Because of their charge neutrality, photons are not defected by intergalactic electric and magnetic fields and therefore point back to the objects emitting them.

Historically, the field of astronomy concerned the study of visible light. The reason for this is visible light is not signifcantly absorbed in the atmosphere. In addition to the visible spectrum, radio waves, some energies of infrared radiation, and long-wavelenth ultraviolet radiation can be measured from the ground. Figure Figure 2.1 shows the transparancy of the atmosphere of the earth to photons of differnet wavelenths.

Slowly, over time, astronomers expanded their view across the electromagnetic spectrum. First, the astronomical observations were made from the ground. Infrared radiation from the sun was first observed by William Herschel in 1800. Herschel

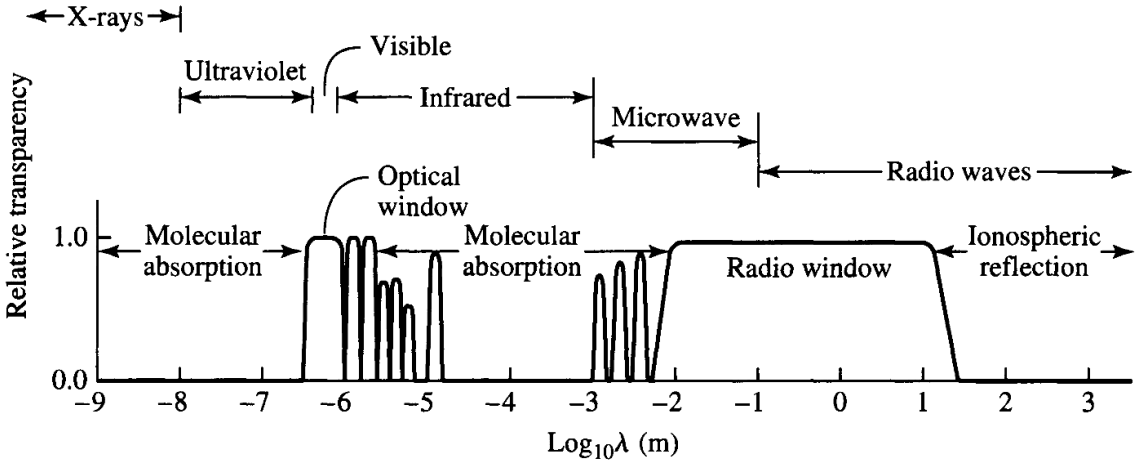

Figure 2.1: Transparency of the atmosphere of the earth to photons of varying wavelenthts. This figure is from Carroll & Ostlie (2006)

measured this infrared radiation by measuring the temperature of sunlight through a prisim and extending the measurement past the red part of the spectrum (Herschel 1800). The first extraterrestrial source of radio waves was detected by Jansky in 1933. Janksy, a radio engineer at Bell labs, was studying the origins of radio interference when he detected radio emission towards the center of our galaxy. (Jansky 1933).

The expansion of the astronomical fronteire to other wavelenths required the development of rockets and sattelites in the 20th ceuntry. The first ultraviolet observation of the sun was performed in 1946 from a captured V-2 rocket (Baum et al. 1946). Observations of solar x-rays were also first carried out on a captured V-2 Rocket in 1949 (Burnight 1949).

2.2 The History of Gamma-ray Astrophysics

It was only natural to wonder about photons with even higher energies. These higher energy photons must come from more extreme processes in space.

As is common in the field of physics, the prediction of the detection of cosmic γ-rays far proceeded their discovery. Feenberg & Primakoff (1948) theorized that

the interaction of starlight with cosmic rays could produce γ-rays through inverse Compoton (IC) upscattering. Following the discovery of the neutral pion in 1949, Hayakawa (1952) predicted that γ-ray emission could be observed from the decay of neutral pions when cosmic rays interacted with interstellar matter. And in the same year, Hutchinson (1952) discussed the bremsstrahlung radiation of cosmic-ray electrons. Morrison (1958) first predicted the detection of several sources of γ-rays including solar flares, pulsar wind nebulae (PWNe), and active galaxies.

Attempts were made in the 1940s and 1950s to determine the composition of cosmic rays using balloon-based experiments. See, for example Critchfield et al. (1952) and Hulsizer & Rossi (1948). But the attempt to observe cosmic γ-rays was hampered by the strong background of atmospheric albedo γ-rays.

The first space-based γ-ray detector was Explorer XI Kraushaar et al. (1965). It was developed at the Massachusetts Institute of Technologys (MITs) under the direction of William L. Kraushaar. Explorer XI incorporated five alternating slabs of cesium iodide and sodium iodide which would induce a gamma-ray to pair-convert into an electron positron pair. The electron and positron pair would then travel through a sandwich scintillation detector. A scintillator is a crystalline material that emits low-energy photons when a high-energy charged particle travels through it. A Cherenkov counter below the scintillation detector measured these low-energy photons, which allowed for the measurement of the energy of the γ-rays. This experiment was surrounded by a plastic anticoincidence scintillation counter which allowed for the rejection of background particles. Figure 2.2 shows the experimental design of Explorer XI.

Explorer XI operated in the energy energy range above 100 MeV. It had an area of $\sim 45\text{cm}^2$ but an effective area of only $\sim 7\text{cm}^2$, corresponding to a detector efficiency of $\sim 15\%$.

It was launched on board Explorer XI on April 27, 1961. The instrument was in operation for 7 months, but only 141 hours of data were of acceptable quality. Using these observations, Explorer XI observed 31 γ-rays and, because the distribution a distribution of these γ-rays was consistent with being isotropic, the experiment could not firmly identify the γ-rays as being cosmic in nature.

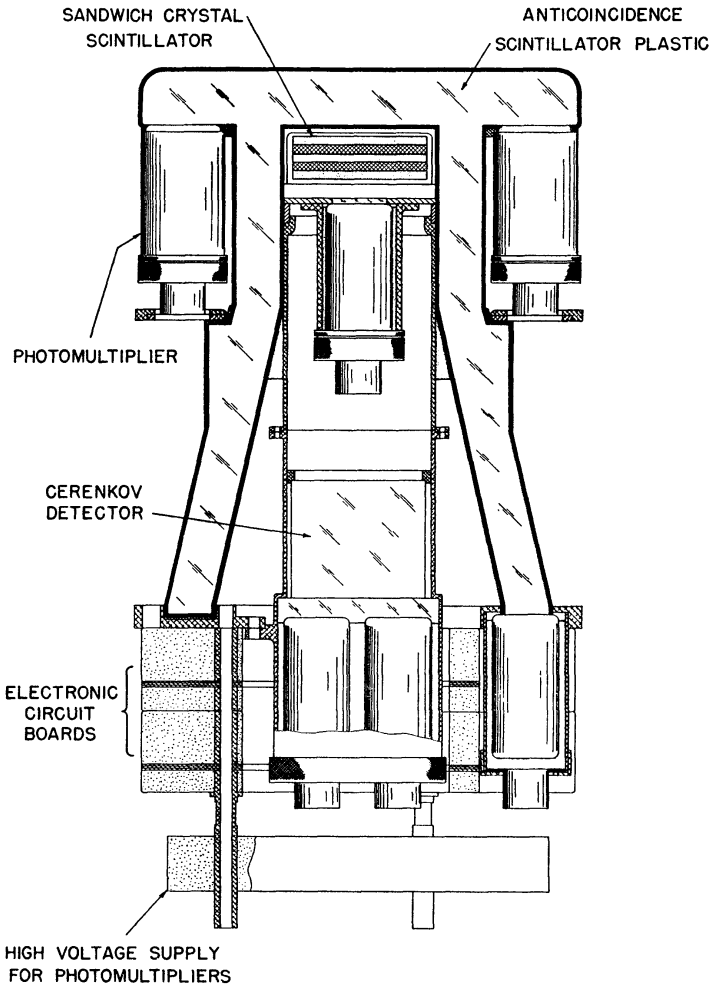

Figure 2.2: The experimental design of Explorer XI. This figure is from Kraushaar et al. (1965).

The first definitive detection of γ-ray came in 1962 by an experiment on the Ranger 3 moon probe (Arnold et al. 1962). It detected an isotropic flux of γ-rays in the 0.5 MeV to 2.1 MeV energy range.

The Third Orbiting Solar Observatory (OSO-3), also developed by Kraushaar, was the next major astrophysical γ-ray detector (Kraushaar et al. 1972). OSO-3 allowed the on board γ-ray detected to have an improved weight, power, telemetry, and exposure, creating a more sensitive experiment. The experiment operated in the energy range from 50 MeV to $\sim$ 400 MeV, had an effective area ~ 9 cm^2, and had a angular resolution of $\sim 24^\circ$ at its full width at half maximum (FWHM).

OSO-3 was launched on March 8, 1967 and operated for 16 months, measuring 621 cosmic γ-rays. The most important result of the experiment was to measure a strong anisotrophy in the distribution of the γ-rays with a strong clustering of γ-rays towards the Galactic plane. Figure 2.2 shows a sky map of these γ-rays. This experiment confirmed both a Galactic component to the γ-ray sky as well as an additional isotropic component, hypothesised to be extragalactic in origin.

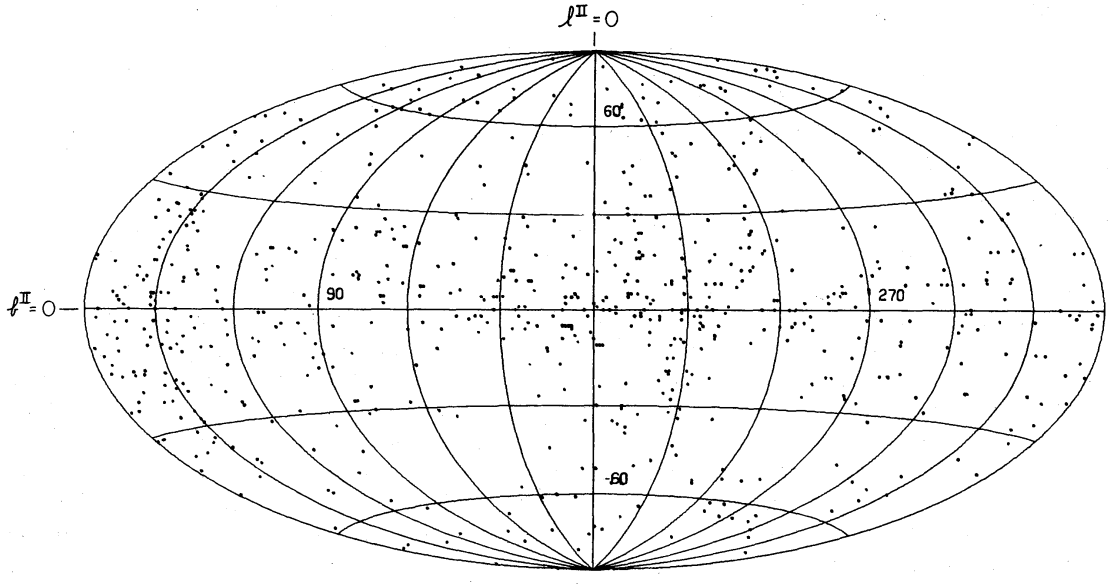

Figure 2.3: The position of all 621 cosmic γ-rays detected by OSO-3. This figure is from Kraushaar et al. (1972).

The major discovery by OSO-3 was confirmed by a balloon-based γ-ray detector in 1970 (Kniffen & Fichtel 1970). In the following year, the first γ-ray pulsar (the Crab) was detected by another balloon-based detector Browning et al. (1971).

The next major advancement in γ-ray astronomy came the second Small Astronomy Satellite (SAS-2) and COS-B.

SAS-2 was a dedicated γ-ray detector launched by the National Aeronautics and Space Administration (NASA) in November 15, 1972. SAS-2 was Fichtel et al. (1975) It improved upon OSO-3 by incorporating a spark chamber and having an overall larger size. The size of the active area of the detector was 640 cm^2 and the experiment had a much improved effective area of $\sim 115\, cm^2$. The spark chamber allowed for a separate measurement of the electron and positron tracks, which allowed for improved directional reconstruction of the incident γ-ray. SAS-2 had a PSF $\sim 5^\circ$ at 30 MeV and $\sim 1^\circ$ at 1 GeV.

SAS-2 collected data for over 6 months before a power supply failure ended data collection. SAS-2 Observed over 8,000 γ-ray photons covering $\sim$ 55% of the sky including most of the Galactic plane. SAS-2 discovered strong emission along the Galactic plane and particularly towards the Galactic cente. It also discovered pulsations from the Crab (Fichtel et al. 1975) and Vela pulsar (Thompson et al. 1977b). In addition, SAS-2 discovered Geminga, the first γ-ray source with no compelling multiwavelenth counterpart (Thompson et al. 1977a). Gemina was eventually discovered to be a pulsar by the Energetic Gamma Ray Experiment Telescope (EGRET) (Bertsch et al. 1992) and retroactively by SAS-2 (Mattox et al. 1992).

on August 9, 1975, the European Space Agency (ESA) launched COS-B, a γ-ray detector similar to SAS-2. COS-B included a spark chamber but improved upon the design of SAS-2 by including a calorimeter below the spark chamber which improved the energy resolution to $< 100\%$ for energies $\sim 3\,\mathrm{GeV}$ (Bignami et al. 1975). COS-B has a comparable effective area to SAS-2: $\sim 50\,\mathrm{cm}^2$ at $\sim 400\,\mathrm{MeV}$ (Bignami et al. 1975).

COS-B operated successfully for over 6 years and produced the first detailed catalog of the γ-ray sky. In total, COS-B observed $\sim 80,000$ photons Mayer-Hasselwander et al. (1982). The second COS-B catalog (2CG) detailed the detection 25 γ-ray sources

for $E > 100\,\mathrm{MeV}$ (Swanenburg et al. 1981). Figure 2.2 shows a map of these sources. Of these sources, the vast majority lay along the galactic plane and could not be positively identified with sources observed at other wavelengths. In addition, COS-B observed the first ever extragalactic γ-ray source, (3C273, Swanenburg et al. 1978).

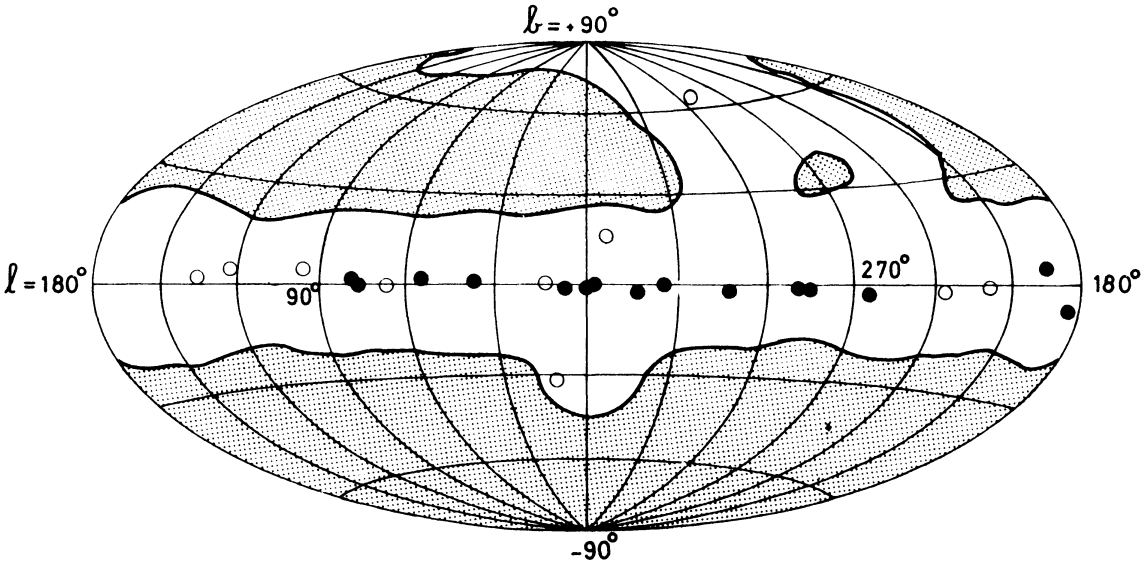

Figure 2.4: A map of the sources observed by COS-B. The filled circles represent brighter sources. The unshaded region corresponds to the parts of the sky observed by COS-B. This figure is from Swanenburg et al. (1981).

The next major γ-ray experiment was EGRET. It was launched on board the Compton Gamma Ray Observatory (CGRO) in April , 1991. CGRO was second of the Great Observatories satellites launched by NASAs. EGRET had a design similar to SAS-2, but had an expanded energy range, operating from 20 MeV to 30 GeV, an improved effective area of $\sim 1500\,\mathrm{cm}^2$ from $\sim$ 500MeV to $\sim 1\,\mathrm{GeV}$, and an improved angular resolution, decreasing to $\sim 0.5^\circ$ at its highest energies Thompson et al. (1993).

At the time, CGRO was the heaviest astrophysical experiment launched into orbit, weighting $\sim 17,000\,\mathrm{kg}$. EGRET contributed $\sim 6,000\,\mathrm{kg}$ to the mass of CGRO.

EGRET vastly expanded the field of γ-ray astronomy. EGRET detected six pulsars (Nolan et al. 1996) and also the Crab Nebula Nolan et al. (1993). EGRET also detected the LMC, the first normal galaxy outside of our galaxy to be detected at

γ-rays (Sreekumar et al. 1992). EGRET also detected Centarus A, the first radio galaxy detected at γ-rays Sreekumar et al. (1999). In total, EGRET detected 271 γ-ray sources using 4 years. The results were presentted in the Third EGRET Catalog (3EG) (Hartman et al. 1999). This catalog included 66 high confidence blazar identifications and 27 low-confidence AGN identifications. Figure 2.2 plots the position of the sources observed by EGRET.

In total, EGRET detected over 1,500,000 celestial gamma rays Thompson (2008).

EGRET was designed with a 2 year mission lifetime, but operated for 9 years. Over time, the performance of EGRET degraded due to hardware failure and due to having to replenish gas in the spark chamber Esposito et al. (1999).

Get a picture of EGRET to include

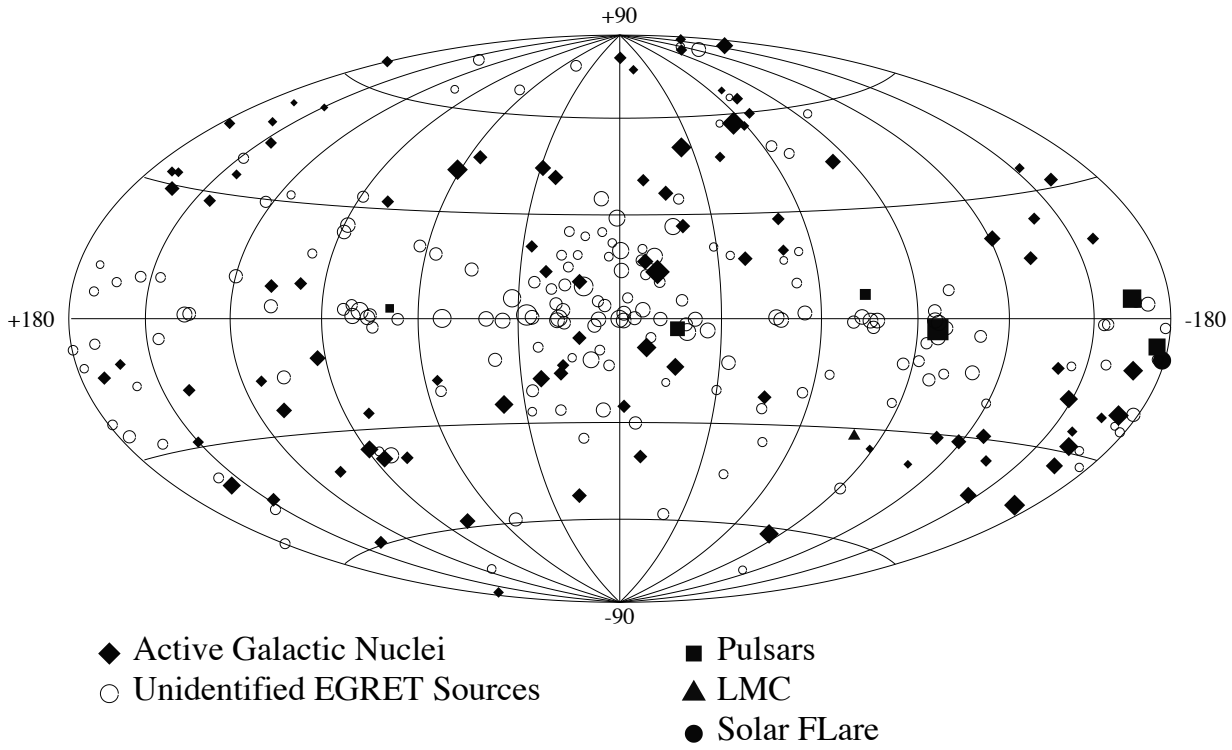

Figure 2.5: The position of EGRET sources in the sky in galactic coordinates. The size of the source markers corresponds to the overall source intensity. This figure is from (Hartman et al. 1999).

- AGILE
- *Fermi*
- Short description of the history of TeV astronomy
- A detailed description of *Fermi* detector will be presented in Section 2.3.4.
- The major source classes detected by *Fermi* will be presented in Section 2.7

  The principles of the detector will be described in Section 2.3.4.

  What is the LAT effective area?

2.3 The *Fermi* Gamma-ray Space Telescope

The Large Area Telescope (LAT) is a pair-production telescope

2.3.1 The Tracker

2.3.2 The Calorimiter

2.3.3 Anti-Coincidence Detector

The Anti-Coincidence Detector (ACD) is ...

2.3.4 Gamma-ray Burst Monitor

2.4 Astrophysical Sources of Gamma-rays

2.4.1 Pulsars

"The gravitational collapse of the core of a massive star into a neutron star (e.g., Baade & Zwicky 1934) releases enough energy to power a supernova explosion (e.g., Zwicky 1938)." – gelfand_2009_dynamical-model

"First widely accepted prediction of an ultra-dense star was given by Zwicky and Baade (1934). Proposed the idea that a supernova represents the transition of an ordinary star into a neutron star, consisting mainly of neutrons." – `http://www.atnf.csiro.au/research/pulsar/orange10/pdf/RaiYuenOrange2010.pdf`

Pulsars were first discovered in 1967 by Jocelyn Bell Burnell and Antony Hewish (Hewish et al. 1968). They had constructed a radio telescope that used interplanetary scintillation wiht the intention of observing quasars. In the process, they detected a source with a periodicity of 1.3 s.

Make note of "Air force had early warning of pulsars" paper

Even before the discovery, Pacini (1967) had predicted the existence of neutron stars (NSs). Shortly following the 1967 discovery, Gold (1968) and Pacini (1968) argued that the observed pulsar was a rotating NS.

The discovery of many more pulsars came quickly. In 1968, and the Vela pulsar (Large et al. 1968) and the Crab pulsar (Staelin & Reifenstein 1968) were discovered.

The first pulsar observed at optical frequencies was the Crab, discovered in 1969 shortly after its radio discvoery (Cocke et al. 1969). In the same year, the first X-ray pulsations were discovered from the same source. At the time, there were no space-based X-ray observatories, so observations had to be performed from rockets. The discovery was carried out almost concurrently by a group at the Naval Research Laboratory (NRL) (Fritz et al. 1969) and at MIT (Bradt et al. 1969). Using proportional counters, these experiments showed that the pulsed emission from the Crab extended to X-ray energies and that, for this source, the X-rays emission was a factor > 100 more energetic than the observed visible emission.

- I read somewhere, but don't have the reference (it was one of htose verbose history books on pulsars), that originally the neutron star hypothesis wasn't well accepted. But then one pulsar was found with a very short period (I think the Crab) which, for causaility reasons, had to be small enough taht it seemed to confirm the Neutron star hypotehsis.

- For Crab describe spin down?: "and these pulsations were then shown to be slowing down at a rate of 36 ns per day (Richards & Comella 1969)." – Gaensler

& Slane (2006)

As was discussed in Section 2.2, γ-ray emission from the Crab was detected only 2 years later (Browning et al. 1971).

First gamma-ray detection

ATNF catalog?

- "There are currently more than 1,800 pulsars in the ATNF on-line catalog [Manchester et al., 2005], with rotation periods in the rage 0.0016-12 seconds (Figure 3.1) and derived spin down luminosities in the range XXX - XXX erg/s." – dalton_2011_identication-gamma-ray

EGRET pulsars?

The state of the art in γ-ray detection of pulsars will be included in an upcomming pulbication. 2PC: Section 2.7.2

When was the PSR, PWN connection made

2.4.2 Pulsar Wind Nebulae

A PWN is a diffuse nebula of shocked relativistic particles. A PWNs surrounds and is powered by an accompanying pulsar. PWNs have been observed long before the discovery of pulsars, but the pulsar/PWN connection could not be made until after the detection of pulsars.

The most famous PWNs is the Crab nebula, associated with the Crab pulsar.

- Chinese SN observations of Crab Nebulae: (p128 of "The Crab Nebula: An Astrophysical Chimera") "It was probably also recorded by Anasazi Indian artists (in present-day Arizona and New Mexico), as findings in Navaho Canyon and White Mesa (both Arizona) as well as in the Chaco Canyon National Park (New Mexico) indicate; there's a review of the research on the Chaco Canyon Anasazi art online. In addition, Ralph R. Robbins of the University of Texas has found Mimbres Indian art from New Mexico, possibly depicting the supernova." – http://messier.seds.org/m/m001.html

It was discovered in 1731 by physician and amateur astronomer John Bevis. This source was going to be published in his sky atlas *Uranographia Britannica*, but the work was never publisehd because his published filed for bankrupcy in 1950. Figure Figure 2.4.2 shows Beavis' plate containing the Crab nebula. A detailed history of John Bevis' work can be found in Ashworth (1981).

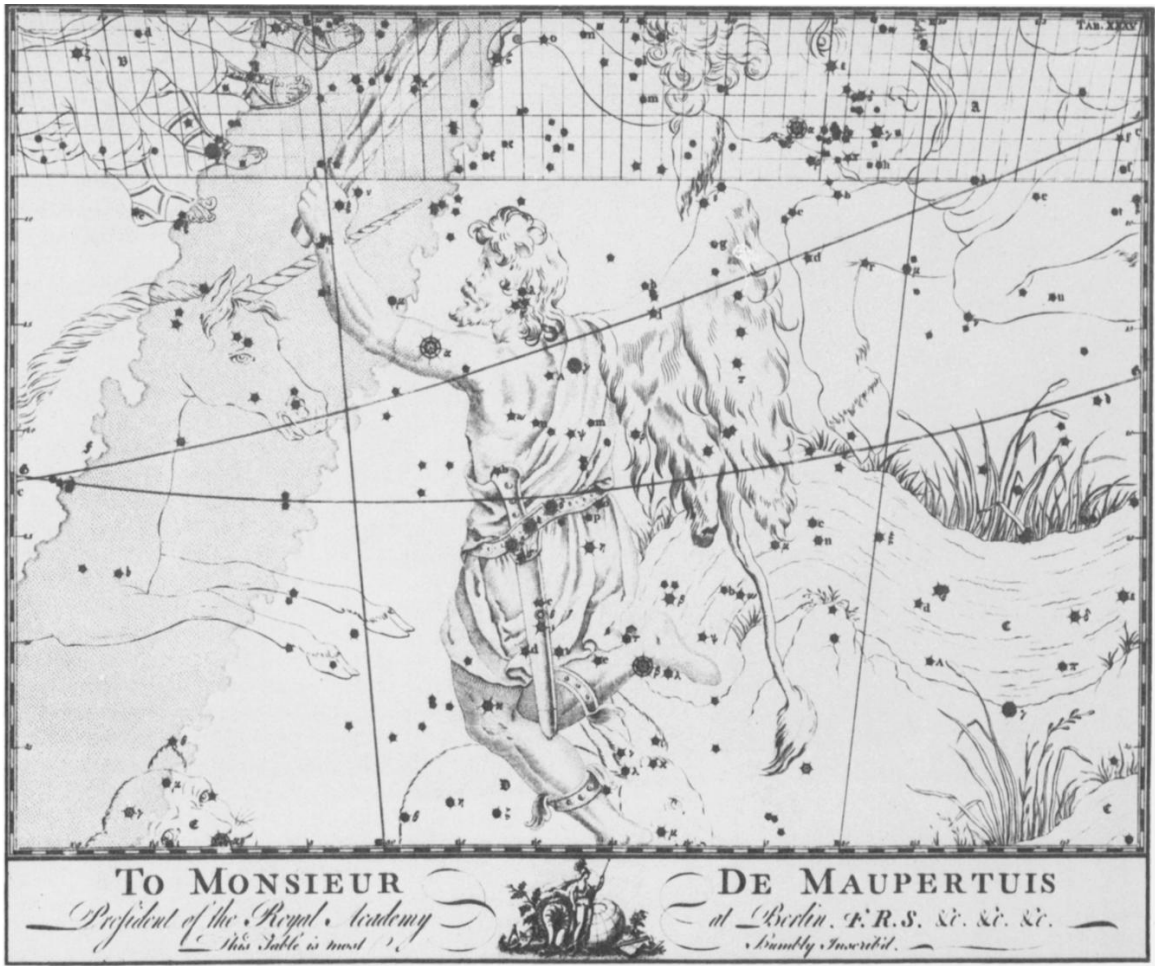

Figure 2.6: The Orion plate from Bevis' book *Uranographia Britannica*. The Crab nebula can be found on the horn of Taurus the Bull on the top of the figure and the source is marked by a cloudy symbol. This figure was reproduced from Ashworth (1981).

- Crab Nebulae is M1 in Charles Messier's catalog 1758 (p128 of "The Crab

Nebula: An Astrophysical Chimera")

- Connection to 1054: "Lundmark (1921) suggested a connection between the Crab Nebula and the event of 1054 AD" (p128 of "The Crab Nebula: An Astrophysical Chimera") "The Crab Nebula (Fig. 1) is almost certainly associated with a supernova (SN) ex- plosion observed in 1054 CE (Stephenson & Green 2002, and references therein)." – "The Evolution and Structure of Pulsar Wind Nebulae" Bryan M. Gaensler and Patrick O. Slane

- "The same year, J.C. Duncan of Mt. Wilson Observatory compared photographic plates taken 11.5 years apart, and found that the Crab Nebula was expanding at an average of about 0.2" per year; backtracing of this motion showed that this expansion must have begun about 900 years ago (Duncan 1921). Also the same year, Knut Lundmark noted the proximity of the nebula to the 1054 supernova (Lundmark 1921)." – http://messier.seds.org/m/m001.html "In 1942, based on investigations with the 100-inch Hooker telescope on Mt. Wilson, Walter Baade computed a more acurate figure of 760 years age from the expansion, which yields a starting date around 1180 (Baade 1942); later investigations improved this value to about 1140. The actual 1054 occurrance of the supernova shows that the expansion must have been accelerated." – http://messier.seds.org/m/m001.html

- "but it was not until 1942 that Duyvendak (1942) and Mayall & Oort (1942) presented complete studies of modern observations of the expanding nebula and of the early Chinese records. It was this work that established unambiguously that the Crab is the remnant of SN1054." (p128 of "The Crab Nebula: An Astrophysical Chimera")

- "1949, the Crab nebula was identified as a strong source of radio radiation (Bolton et.al. 1949), discovered 1948 named and listed as Taurus A (Bolton 1948), and later as 3C 144." - http://messier.seds.org/m/m001.html

- Synchrotron emission hypotehsis: "while the inner, blueish nebula emits continuous light consisting of highly polarised so-called synchrotron radiation, which is

emitted by high-energy (fast moving) electrons in a strong magnetic field. This explanation was first proposed by the Soviet astronomer J. Shklovsky (1953) and supported by observations of Jan H. Oort and T. Walraven (1956)." – http://messier.seds.org/m/m001.html

- "X-rays from this object were detected in April 1963 with a high-altitude rocket of type Aerobee with an X-ray detector developed at the Naval Research Laboratory; the X-ray source was named Taurus X-1. Measurements during lunar occultations of the Crab Nebula on July 5, 1964, and repeated in 1974 and 1975, demonstrated that the X-rays come from a region at least 2 arc minutes in size, and the energy emitted in X-rays by the Crab nebula is about 100 times more than that emitted in the visual light" – http://messier.seds.org/m/m001.html

- Association of Crab pulsar with Crab nebulae were discussed in (Staelin & Reifenstein 1968).

- "Just after discovery of pulsars, Gunn & Ostriker (1969) suggested that particles can be accelerated to very high energies in the pulsar wind zone." – "Relativistic Astrophysics and Cosmology" by Shapiro

- TEV observations of Crab. brightest soruce in the sky...

- Now many radio, x-ray PWNe. Count form PWN catalog: http://www.physics.mcgill.ca/ pulsar/pwncat.html "Observations over the last several decades have identified 40 to 50 further sources, in both our own Galaxy and in the Magellanic Clouds, with properties similar to those of the Crab Nebula (Green 2004; Kaspi, Roberts & Harding 2006)" – Gaensler & Slane (2006)

- How many TeV PWNe in TeVCat? http://tevcat.uchicago.edu/ (31 by my preliminary count)

2.5 Radiation Processes in Gamma-ray Astrophysics

XXXXXXXXXXXXXXXXXXXXXXXXXXXXXXXXXXXXXXXXXXXXXXXXXXXXXXXX

- The non-thermal radiation processes typical in astrophysics are most comonly

2.5.1 Synchrotron

Charged particles in magnetic fields experince an electromagnetic force:

$$\frac{\mathrm{d}}{\mathrm{d}t}(\gamma m\boldsymbol{v}) = \frac{q}{c}\boldsymbol{v}\times\boldsymbol{B} \tag{2.1}$$

The energy output per unit frequency due to syncrotron radiation is

$$P(\omega) = \frac{\sqrt{3}q^3 B\sin\alpha}{2\pi mc^2}F(x) \tag{2.2}$$

Where

$$F(x) \equiv x\int_x^\infty K_{\frac{5}{3}}(\eta)d\eta \tag{2.3}$$

and

$$x \equiv \omega/\omega_c \tag{2.4}$$

and

$$\omega_B = \frac{qB}{\gamma mc} \tag{2.5}$$

We assume a particle distribution of electrons, written The electron spectrum is often

$$N(E)\mathrm{d}E = CE^{-\gamma}\mathrm{d}E \tag{2.6}$$

The total power output per unit frequency

$$P(\omega) = \int P(\omega)N(E)\mathrm{d}E \tag{2.7}$$

2.5.2 inverse Compoton

Why don't protons syncrotron radiate?

IC emission is ...

2.5.3 Bremsstrahlung

Why no Bremsstrahlung radiation from PWN. Maybe a back-of-the-eveolope estimate

2.5.4 Pi0 Decay

Describe the characteristic pi0 cutoff energy

2.6 The Galactic Diffuse and Isotropic Gamma-ray Background

Include discussion of modeling, if time permitting

- Discuss the historical Observations of galactic diffuse emission

  Mention how OSO-3 first detected the *gamma*-rays from the galaxy: Section 2.2.

- GALPROP model of diffuse emission. Reference: `http://arxiv.org/abs/1202.4039`
- Emperical Ring model of galactic diffuse emisson.
- The isotropic background: `http://arxiv.org/abs/1002.3603`
- Galactic diffuse emission is primarily composed of ...
- Something about how great galprop is.
- Something about

2.7 Sources Detected by the Fermi the Large Area Telescope

- A variety of sources detected by the The Large Area Telescope:

2.7.1 The Second Fermi Catalog

The second *Fermi* catalog (2FGL) was a catalog by the LAT collaboration containing XXX Sources.

Describe Catalog

- Citation is Nolan et al. (2012)
- Source classification method
- Number of sources detected by the LAT
- Forward reference Chapter 4, which does a more thorough description of likelihood analysis method.
- Source classes/associations

2.7.2 The Second Fermi Pulsar Catalog

The second *Fermi* pulsar catalog (2PC) is a ...

- Process of detecting Pulsars with the LAT
- Number of pulsars detected by the LAT

2.7.3 Pulsar Wind Nebulae Detected by The Large Area Telescope

Crab

Vela X

MSH 15-52

Dig up HESS reference of HESS J1514-59.

HESS J1825−137

HESS J1825−137 is a cool source

HESS Detection: HESS Energy dependent morphology: Aharonian et al. (2006a)

LAT Detection: Grondin et al. (2011)

HESS J1640−465

HESS J1640−465 is also cool.

HESS detection: Aharonian et al. (2006b) Fermi detection: Slane et al. (2010)

2FGL J1857+026

2FGL J1857+026 is another good source.

LAT detection: Rousseau et al. (2012)

1. `http://arxiv.org/pdf/1206.3324v1.pdf`

J1023

...

Chapter 3

The Pulsar/Pulsar Wind Nebula System

3.1 Neutron Star Formation

As was discussed in Section 2.4, pulsars, PWNs, and supernova remnants are all the end products of supernovas. When a star undergoes a supernova, the ejecta forms a supernova rememant. If the remaining stellar core has a mass above the Chandrasekhar limit, then the core's electron degeneracy pressure cannot counteract the core's gravitational force and the core will collapse into a NS. The Chandrasekhar mass limit can be approximated as (Chandrasekhar 1931)

$$M_{\mathrm{Ch}} \approx \frac{3\sqrt{2\pi}}{8}\left(\frac{\hbar c}{G}\right)^{3/2}\left[\left(\frac{Z}{A}\right)\frac{1}{m_{\mathrm{H}}^2}\right] \tag{3.1}$$

where $\hbar$ is the reduced Planck constant, c is the speed of light, G is the gravitational constant, m_{H} is the mass of hydrogen, Z is the number of protons, A is the number of nucleons, and $M_{\odot}$ is the mass of the sun. This formula can be found in (Carroll & Ostlie 2006). When this formula is computed more exactly, one finds $M_{\mathrm{Ch}} = 1.44 M_{\odot}$.

Because NSs are supported by a neutron degeneracy pressure, the radius of a

neutron star can be approximated as

$$R_{\rm ns} \approx \frac{(18\pi)^{2/3}}{10} \frac{\hbar^2}{G M_{\rm ns}^{1/3}} \left(\frac{1}{m_{\rm H}} \right)^{8/3} \tag{3.2}$$

This formula can be found in (Carroll & Ostlie 2006). The canonical radius for NSs is $\sim 10\,\mathrm{km}$.

In these very dense enviroments, the protons and electrons in the NS form into neutrons through inverse β decay:

$$p^+ + e^- \rightarrow n + \nu_e. \tag{3.3}$$

But if a NS had a sufficiency large mass, the graviational force would overpower the neutron degeneracy pressure and the object would collapse into a black hole. The maximum mass of a NS is unknown because it depends on the equation of state inside the star, but is comonly predicted to be $\sim 2.5 M_\odot$ Recently, a pulsar with a mass of $\sim 2 M_\odot$ was discovered (Demorest et al. 2010), constrainging theories of the equation of state.

In addition to rotationally-powered pulsars, the primary class of observed pulsars, there are two additional source classes of pulsars with a different mechanism powering the source. The first class is accretion-powered pulsars, also called X-ray pulsars, are a bright and populous source class at X-ray energies. In these sources, the emission energy comes from the accretion of matter from a donor star. See Caballero & Wilms (2012) for a review. The second class is magnetars which have a very strong magnetic field and a relativly slow rotational perioid. In magnetars, the strong magnetic field powers the emission. See Rea & Esposito (2011) for a review.

3.2 Pulsar Evolution

The simplest model of a pulsar is that it is a rotating dipole magnet with the rotation axis and the magnetic axis offset by an angle θ. A diagram of this model is shown in Figure 3.1. The energy output from the pulsar is then assumed to come from

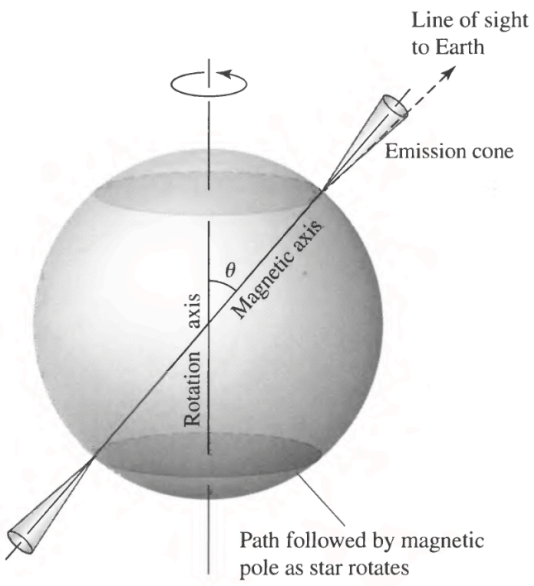

Figure 3.1: The rotating dipole model of a puslar. This figure is taken from (Carroll & Ostlie 2006).

rotational kintetic energy stored in the netutron star which is released as the pulsar spins down.

Both the period P and the period derivative $\dot{P} = dP/dt$ can be directly observed for a pulsar. Except in a few millisecond pulsars (MSPs) which are being sped up through accreition (see for example Falanga et al. (2005)), pulsars are slowing down ($\dot{P} < 0$).

We write the rotational kinetic energy as

$$E_{\text{rot}} = \tfrac{1}{2} I \Omega^2 \tag{3.4}$$

where $\Omega = 2\pi/P$ is the angular frequency of the pulsar and I is the moment of inertia.

For a uniform sphere,

$$I = \frac{2}{5} M R^2 \tag{3.5}$$

Assuming a canonical pulsar as was described in Chapter 3, we find a canonical moment of inertia of $I = 10^{45}\,\text{g}\,\text{cm}^{-2}$.

We make the conection between the pulsar's spin-down energy and the rotational

kinetic energy as $\dot{E} = -\mathrm{d}E_{\mathrm{rot}}/\mathrm{d}t$. Using this, Equation 3.4 can be rewritten as

$$\dot{E} = I\Omega\dot{\omega} \tag{3.6}$$

It is believed that as the pulsar spins down, the this rotational energy is released as pulsed electromagnetic radiation and also as a wind of electrons and positrons accelerated in the magnetic field of the pulsar.

If the pulsar were a pure dipole magnet, its radiation would be described as (Gunn & Ostriker 1969)

$$\dot{E} = \frac{2B^2 R_{\mathrm{NS}}^6 \Omega^4 \sin^2\theta}{3c^3}. \tag{3.7}$$

Combining equations Equation 3.6 and Equation 3.7, we find that for a pure dipole magnet,

$$\dot{\omega} \propto \Omega^3. \tag{3.8}$$

In the few situations in which this relationship has been definitivly measured, this relationship does has not hold. We generalize Equation 3.8 as:

$$\dot{\omega} \propto \Omega^n \tag{3.9}$$

where n is what we call the pulsar breaking index. And we note that Equation 3.9 we can can solve for n by taking the derivative of the equation

$$n = \frac{\Omega\ddot{\omega}}{\dot{\omega}^2} \tag{3.10}$$

The breaking index is hard to measure due to timing noise and glitches in the pulsar's phase. To this date, it has been meausred in eight pulsars (See Espinoza et al. 2011, and references therein), and in all situations $n < 3$. This suggests that there are additional processes besides magnetic dipole radiation that contribute to the energy release (Blandford & Romani 1988).

Equation 3.9 is a Bernoulli differential equation which can be integrated to solve

for time:

$$T = \frac{P}{(n-1)|\dot{P}|}\left(1 - \left(\frac{P_0}{P}\right)^{(n-1)}\right) \tag{3.11}$$

For a canonical $n = 3$ pulsars which is relativly old $P_0 \ll P$, we obtain what is called the characteristic age of the pulsar:

$$\tau_c = P/2\dot{P}. \tag{3.12}$$

Using Equation 3.6 and Equation 3.8, we can solve for the spin-down evolution of the pulsar as a function of time (Pacini & Salvati 1973)

$$\dot{E}(t) = \dot{E}_0\left(1 + \frac{t}{\tau_0}\right)^{-\frac{(n+1)}{(n-1)}} \tag{3.13}$$

where

$$\tau_0 \equiv \frac{P_0}{(n-1)|\dot{P}_0|}. \tag{3.14}$$

Equation 3.9, Equation 3.11, and Equation 3.13 show us that given the current P, $\dot{P}$, $\dot{E}$, P_0, and breaking index n, we can calculate the pulsar's age and energy-emission history.

In a few situations, the pulsar's age is well known and the breaking index can be measured, so P_0 can be infered. See Kaspi & Helfand (2002) for a review of the topic. For other sources, attempts have been made to infer the initial spin-down age based on the dynamics of an associated supernova remnant (SNR)/PWN (van der Swaluw & Wu 2001).

Finally, if we assume dipole radiation is the only source of energy release, we can comibe equation Equation 3.6 and Equation 3.7 to solve for the magnetic field:

$$B = \sqrt{\frac{3Ic^3}{8\pi^2 R_{\rm NS}^6 \sin^2\theta} P\dot{P}} = 3.2 \times 10^{19}\sqrt{P\dot{P}}\,\mathrm{G} \tag{3.15}$$

where in the last step we assumed the canonical values of $I = 10^{45}\,\mathrm{g\,cm^{-2}}$, $R_{\rm NS} = 10\,\mathrm{km}$, $\theta = 90°$, and we assume that P is measured in units of seconds. For example,

for the Crab nebula, $P \approx 33\,\mathrm{ms}$ (Staelin & Reifenstein 1968) and $\dot{P} \approx 36\,\mathrm{ns}$ per day (Richards & Comella 1969) so $B \approx 10^{12}\,\mathrm{G}$.

3.3 Pulsar Magnetosphere

The basic picture of a pulsar magnetosphere was first presented in Goldreich & Julian (1969). The magnetic dipole of the rotating NS creates a quadrupole electric field.

The potential generated by this field is given as (Goldreich & Julian 1969):

$$\Delta\Phi = \frac{B\Omega^2 R_{\mathrm{NS}}^2}{2c^2} \approx 6 \times 10^{12} \left(\frac{B}{10^{12}\,\mathrm{G}}\right) \left(\frac{R_{\mathrm{NS}}}{10\,\mathrm{km}}\right)^3 \left(\frac{P}{1\,\mathrm{s}}\right). \tag{3.16}$$

For NSs, this potential produces magnetic field is much larger than the gravitaional force. Threfore, NS magnetospheres can act as a powerful particle accelerators.

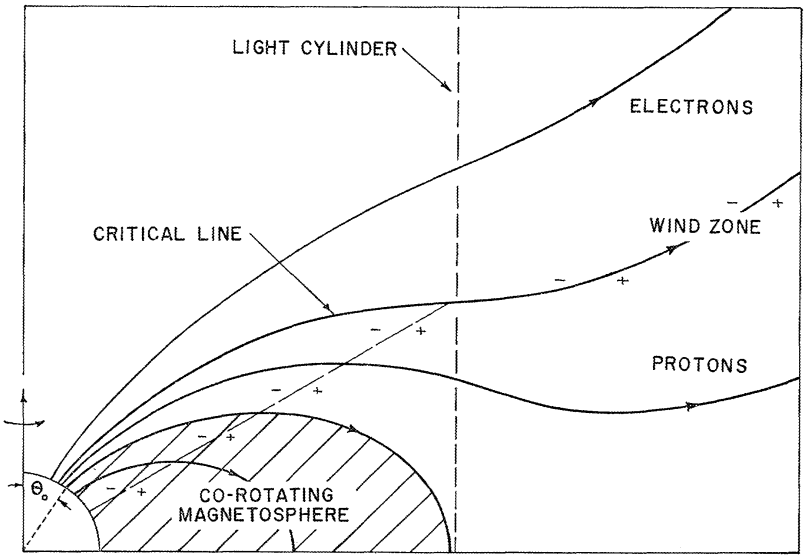

Figure 3.2: The magnetosphere for a rotating pulsar. The pulsar is on the bottom left of the plot. This figure is from Goldreich & Julian (1969).

Figure 3.2 shows a schematic diagram of this magnetosphere.

- Where are sites of acceleratoin

- Charge density in magnetosphere?
- Radio emission
- gamma-ray emission. Slot-gap, outer gap models "A long standing question in pulsar astronomy has been the location of the radio emission. Three places have been suggested; near the light cylinder (Smith 1969), perhaps located in regions of closed magnetic field lines (Gold 1968), and the open field line regions (Radhakrishnan & Cooke 1969). Nowadays, it is widely accepted (see e.g. Lyne & Smith 1990) that the radio emission originates from the open field line region well inside the light cylinder, whereas the very high energy emission (opti- cal and above) probably arises in a quite different mechanism, much nearer to the light cylinder." – kramer_1997a_origin-pulsar

Pulsars typically release only a small percent of their overall energy budget as pulsed emission. The efficiency of converting spin-down energy into pulsed $\gamma-$rays is typically $\sim$ 0.1% to 10% (Abdo et al. (2010b)). For example, the Crab nebulae is estimated to release 0.1% of it's spin-down energy as pulsed γ-rays Abdo et al. (2010a). Typically, the energy released as radio and optical photons is much less. The optical flux of the Crab is a factor of $\sim$ 100 smaller Cocke et al. (1969) and the radio flux is a factor of $\sim 10^4$ smaller. Therefore, the vast majority of the energy output of the pulsar is carried away as a pulsar wind, which will be described in the next section.

3.4 Pulsar Wind Nebulae Structure

The basic picture of the physics of PWNs comes from Rees & Gunn (1974) and Kennel & Coroniti (1984). More and more sophisticated models have emerged over the years. See, for example, Gelfand et al. (2009) and refernces therein.

The wind ejected from the pulsar's magnetosphere is initially cold which means that it flows radially out from the pulsar. This unshocked pulsar wind only emittts radiation through IC Bogovalov & Aharonian (2000). This pulsar wind forms a bubble

as it presses into the SNR and forms a shock where the particle wind is furthere accelerated.

As the wind leaves the magnetosphere, it is believed to be dominated by the energy carried off in electromagnetic fileds (the pointing flux $F_{E\times B}$). The rest of the energy is released as a particle flux ($F_{\rm particle}$). We define the magnetization of the pulsar wind as

$$\sigma = \frac{F_{E\times B}}{F_{\rm particle}} \tag{3.17}$$

"Between the pulsar light cylinder and the position of the wind termination shock the nature of the wind must thus change dramatically, although the mechanism for this transition is as yet unclear (see Arons 2002, Melatos 1998)."

The radius of the bubble ($r_{\rm ts}$) is the radius where the ram pressure from the wind equals the pressure of the gas in the SNR. The ram pressure is computed as the energy in the bubble $\dot{E}r_{\rm ts}/c$ (assuming the particles travel with a velocity $\approx c$) divided by the volume $4\pi r_{\rm ts}^3/3$:

$$r_{\rm ts} = \sqrt{\frac{\dot{E}}{\frac{4}{3}\pi P_{\rm ISM} c}}. \tag{3.18}$$

Here, $P_{\rm ISM}$ is the pressure in the SNR. Typical values for the termination shock are 0.1 pc which is an angular size $\sim$ second of arc (arcsec) for distances $\sim$ kpc (Gaensler & Slane 2006).

At the termination shock, the particles are thermalized (given a random pitch angle), and accelerated to energies of 10^{15} eV (Arons 1996).

Downstream of the shock, the particles emit synchotron and IC radiation as the thermalized electron population interacts with the magnetic filed and seed photons (Gaensler & Slane 2006).

Figure 3.3 shows a diagram describing magnetosphere, unshocked wind, and synchrotron nebula which make up the Pulsar/PWN system.

- "Following this discovery, a theoretical understanding was soon developed in which the central pulsar generates a magnetized particle wind, whose ultrarelativistic electrons and positrons radiate synchrotron emission across the electromagnetic spectrum (Pacini & Salvati 1973, Rees & Gunn 1974). The pulsar has

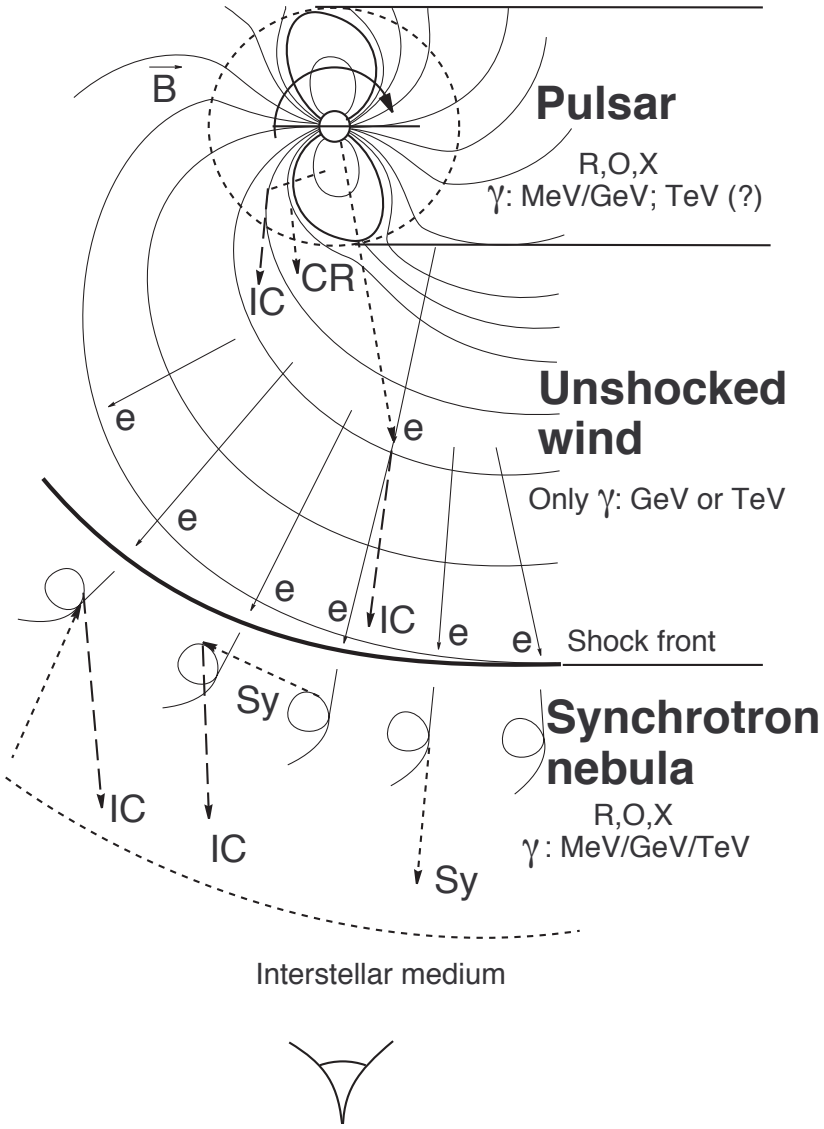

Figure 3.3: The regions of emission in a pulsar/PWN system. This figure shows (top) the pulsar's magnetopshere, (middle), the unshocked pulsar wind and (bottom) the shocked pulsar wind which can be observed as the PWN. "R", "O", "X", and "γ" describe sites of radio, optical, X-ray, and γ-ray emission respectivly. "CR", "Sy", and "IC" refer to regions of curvature, inverse Compton, and synchrotron emission. Figure is taken from Aharonian & Bogovalov (2003).

steadily released about a third of its total reservoir of ???? ergs of rotational energy into its surrounding nebula over the last 950 years. This is in sharp contrast to shell-like SNRs, in which the dominant energy source is the ??? ergs of kinetic energy released at the moment of the original SN explosion." – Gaensler & Slane (2006)

- How is pulsar outflow accelerated at shock?
- Discuss magnetization stuff :
    1. see page 76 in "Relativistic Astrophysics and Cosmology" by Shapiro

Discuss pulsar evolution "The Evolution and Structure of Pulsar Wind Nebulae" – Bryan M. Gaensler and Patrick O. Slane

Describe Mattana's work on PWNs: "On the evolution of the Gamma- and X-ray luminosities of Pulsar Wind Nebulae"

"As has been discussed, pulsar wind nebulae are prominent sources of very high energy -rays. At these wavelengths, emission is caused by inverse Compton acceleration of seed photons by the relativistic electrons present in the nebula (see Section 1.3.5). As the electron energies needed to boost photons to these energies are not as large as that required for synchrotron emission to occur, inverse Compton emission is seen at the extremes of the nebula where synchrotron emission can no longer be observed and as such older pulsar wind nebulae are observed to be much larger in VHE -rays than their X-ray counterparts. In addition to this, inverse Compton emission is seen in the unshocked wind area of the PWN as the electrons present are energetic enough to produce inverse Compton radiation even if they are unable to produce synchroton radiation" – keogh_2010_search-pulsar

"The morphology of a young PWN is often elongated along the pulsar spin axis due to the higher equatorial pressure associated with the toroidal magnetic field (Begelman & Li 1992, van der Swaluw 2003). This effect is seen clearly in many PWNe (e.g., Figs. 1 & 5) and allows one to infer the likely projected orientation of the pulsar. As the nebula expands (see 3.1), Rayleigh-Taylor instabilities form as the fast-moving relativistic fluid encounters and accelerates slower-moving unshocked

supernova ejecta. These form dense, finger-like fillamentary structures that suffer photoionization from the surrounding synchrotron emission and radiate recombination lines in the optical and ultraviolet (UV) bands (Fig. 1(b); Hester et al. 1996). The increased density compresses the magnetic eld around the fillaments, causing enhanced synchrotron emission. One thus observes radio structures that correspond to the optical/UV fillaments." – `http://arxiv.org/pdf/astro-ph/0601081v1.pdf`

Describe SNR Reverse Shock

"In later stages the PWN interacts with the reverse shock formed in the SNR in which the NS was born. This interac- tion causes the disruption of the PWN, often leading to composite SNRs with complicated PWN structures in their interiors." – slane_2005_young-neutron

"The structure of a PWN can be altered significantly through interaction with the reverse shock from the SNR in which it resides. In its early evolution the PWN is basically freely-expanding, encountering only small amounts of slow- moving ejecta in the SNR interior. As the SNR blast wave sweeps up sufficient amounts of circumstellar/interstellar material, a reverse shock is driven back through the ejecta. As this reverse shock propagates, heating the ejecta, it will eventually reach the PWN." – slane_2005_young-neutron

3.5 Pulsar Wind Nebula Emission

In the Pulsar/PWN model, a population of electrons is emitted from the magnetosphere, released as an unshocked wind, and then accelerated at the termination shock. In the surrounding nebula, the electrons emmit synchotron and inverse Compton

- What is the characteristic synchotron energy
- What is the characteristic IC energy
- look at: etten_2012a_particle-populations

Energetics of PWNe:

"The efficiency of conversion of spin-down luminosity into synchrotron emission is defined by efficiency factors and LX/E Typical values are and (Becker & Trumper 1997, Frail & Scharringhausen 1997), although wide excur- sions from this are observed. Note that if the synchrotron lifetime of emitting particles is a significant fraction of the PWN age (as is almost always the case at radio wavelengths, and sometimes also in X-rays), then the PWN emission represents an integrated history of the pulsas spin down, and R and X are not true instantaneous efficiency factor" –gaensler_2006_evolution-structure

X-ray energetics tabulated from: `http://arxiv.org/pdf/astro-ph/0006030v1.pdf`

Chapter 4

Maximum-likelihood analysis of LAT data

In this chapter, we discuss maximum-likelihood analysis, the principle analysis method used to perform spectral and spatial analysis of LAT data. In Section 4.1, we discuss the reasons necessary for employing this analysis procedure compared to other simpler analysis methods. In Section 4.2, we describe the benefits of a maximum-likelihood analysis. In Section 4.3, we discuss the steps invovled in defining a complete model of the sky, a necessary part of any likelihood analysis.

In Section 4.5, we discuss the standard implementation of binned maximum likelihood in the LAT Science Tools and in particular the tool `gtlike`. In Section 4.6, we then discuss the `pointlike` pacakge, an alterate package for maximum-likelihood analysis of LAT data. We discuss the similarities and differences between `pointlike` and `gtlike`.

In the next chapter (Chapter 5), we will discuss the addition of capability into `pointlike` for studying spatially-extended sources and the analysis method which will be used in this paper to study spatially-extended sources.

We not that much of the notation and formulation of likelihood analysis in this chapter follows Kerr (2010).

4.1 Motivations for Maximum-Likelihood Analysis of Gamma-ray Data

Traditonally, spectral and spatial analysis of astrophysical data relies on a process known as aperture photometry. In this process, a source in the data is analyzed by directly measuring the number of photons coming from the object. This process is done by measuring the counts within a given radius of the source and subtracting from it a background level estimated from a nearby region. Often, the source's flux is calibrated by measurements of nearby objects with known fluxes. Otherwise, the flux can be obtained from by dividing the number of counts from the source by the telesocpe's size, the observation time, and the telescope's conversion efficiency.

Similarly, for faint sources the statistical significance of the detection can be obtained from the Poission nature of the data. For TeV experiments such as H.E.S.S., this analysis method is described in Li & Ma (1983).

Unfortunately, this simpler analysis method is inadequate for dealing with the complexities introduced in analyzing LAT data.

Most importantly, aperture photometry assumed that the background is istropic so that the background level below the source can be estimated from nearby regions. As was discussed in Section 2.6, the Galactic diffuse emission is highly anistropic, rendering this assumption invalid.

In addition, this method is not optimal due to the high density of sources detected in the Gamma-ray sky. 2FGL reported on the detection of 1873 sources, which corresponds to an average source spacing of $\sim 5^\circ$. But within the inner 45° of the galactic plane in longitude and 0.5° of the galactic plane in latitidue, there are 73 sources, corresponding to a source density of ~ 1 source per square degree. The aperature photometry method is unable to effecitvly fit multiple sources when the tails of the PSF overlap and furthermore make background estimation problematic.

Finally, this method is suboptimal due to the large energy range of LAT observations. A typical spectral analysis studies a source from an energy of 100 MeV to energies above 100 GeV. Similarly, as was shown in , the PSF of the LAT is rather broad ($\gtrsim 1^\circ$) at low energy and much narrower ($\sim 0.1^\circ$) at higher energies. Therefore,

what section discusses energy

there is a much higher sensitivty to the higher energy photons coming from a source. But simple aperture photometry method would ignore this improvement by weighting each photon equally.

4.2 Description of Maximum-Likelihood Analaysis

The field of γ-ray astrophysics has generally found maximum-likelihood to be a dependable method to avoid the issues discussed above. The term likelihood was first introduced by Fisher (1925). Maximum-likelihood was applied to photon-counting experiments in the context of astrophysics by Cash (1979). Mattox et al. (1996) described the maximum-likelihood analysis framework devoped to analyze EGRET data.

In the formulation, one relies upon primarily upon the likelihood function. The likelihood, denoted $\mathcal{L}$, is quite simply the probability of obtaining the observed data given an assumed model:

$$\mathcal{L} = P(\text{data}|\text{model}) \tag{4.1}$$

Section 4.3 will provide describe the components that go into a model of the data.

Generaly, a model of the sky depends upon a list of parameters that we denote as $\boldsymbol{\lambda}$. Therefore, the likelihood function itself becomes a function of the parameters of the model:

$$\mathcal{L} = \mathcal{L}(\boldsymbol{\lambda}) \tag{4.2}$$

The term maximum-likelihood refers to the fact that the best-fit parameters of a model can be estimated by maximizing the likelihood function.

What are the benefits of maximum likelihood

Describe Wilk's Therorem and it's application to parameter error estimation

4.3 Defining a Model of the Sources in the Sky

In order to perform a maximum-likelihood analysis, one requires a parameterized model of the sky. A model of the sky is composed of a set of γ-ray sources, each

characterized by its photon flux density $\mathcal{F}(E, t, \vec{\Omega}|\boldsymbol{\lambda})$. This represents the number of photons emitted per unit energy, per unit time, per units solid angle at a given energy, time, and position in the sky. In the Centimetre-Gram-Second System of Units (CGS), it has units of ph $\mathrm{cm}^{-2}\mathrm{s}^{-1}\mathrm{erg}^{-1}\mathrm{sr}^{-1}$.

Often, the spatial and spectral part of the source model are separable and independent of time. When that is the case, we like to write the source model as

$$\mathcal{F}(E, t, \vec{\Omega}|\boldsymbol{\lambda}) = \frac{dN}{dE} \times \mathrm{PDF}(\vec{\Omega}). \tag{4.3}$$

Here, $\frac{dN}{dE}$ is only a function of energy and PDF $(\vec{\Omega})$ is only a function of position $(\vec{\Omega})$. In this formulation, some of the model parameters $\boldsymbol{\lambda}$ are taken by the $\frac{dN}{dE}$ function and some by the PDF$(\vec{\Omega})$ function. In CGS, $\frac{dN}{dE}$ is in units of ph $\mathrm{cm}^{-2}\mathrm{s}^{-1}\mathrm{erg}^{-1}$.

The spectrum $\frac{dN}{dE}$ is typically modeled by simple geometric functions. The most popular spectral model is a power law (PL):

$$\frac{dN}{dE} = N_0 \left(\frac{E}{E_0}\right)^{-\gamma} \tag{4.4}$$

Here, $\frac{dN}{dE}$ is a function of energy and also fo the two model parameters (the prefactor N_0 and the spectral index γ). The parameter E_0 is often called the energy scale or the pivot energy and is not considered a model parameter.

Another common spectral model is the broken-power law (BPL) spectral model

$$\frac{dN}{dE} = N_0 \times \begin{cases} (E/E_b)^{-\gamma_1} & \text{if } E < E_b \\ (E/E_b)^{-\gamma_2} & \text{if } E \geq E_b \end{cases} \tag{4.5}$$

This model represents a powerlaw with an index of γ_1 which has a break at energy E_b to having an index of γ_2.

Finally, the exponentially-cutoff power law (ECPL) spectral model is often used to model the γ-ray emission from pulsars:

$$\frac{dN}{dE} = N_0 \left(\frac{E}{E_0}\right)^{-\gamma} \exp\left(-\frac{E}{E_c}\right). \tag{4.6}$$

For energies much below E_c, the ECPL is a PL with spectral index γ. For energies much larger than E_c, the ECPL exponentially decreases.

PDF represents the spatial distribution of the emisison. It is traditionally normalized as though it was a probability:

$$\int d\Omega \, \mathrm{PDF}(\vec{\Omega}). \tag{4.7}$$

Therefore, in CGS PDF has units of sr^{-1} For a point-like source at a position $\vec{\Omega}'$, the spatial model is:

$$\mathrm{PDF}(\vec{\Omega}) = \delta(\vec{\Omega} - \vec{\Omega}') \tag{4.8}$$

and is a function of the position of the source. Example spatial models for spatially-extended sources will be presented in section XXXXX

This formulation assumed that the source models are not time dependent. This is traditionally because it is difficult to find simple paremterized models to fit the time behavior of a variable source. Instead, the typtical strategy to fit varaible sources is to divide a large range of time into multiple smaller time intervals and to perform multiple likelihood fits in each time range.

In some situations, the spatial and spectral part of a source do not nicely decouple. An example of this could be SNRs which could show a spectral variation across the source. Katsuta et al. (2012) and Hewitt et al. (2012) have simplied this problem by A simple method which has been adopted to study this kind of sourcc.

FINISH DISCUSSION

In situations where spatial and spectral components couple, typical to make multiple spatial templates, each with an indepdnet spectra (e.g. the Puppis A paper's fitting multiple hemispheres).

Discuss how diffuse background is more complciated and requires a mapcube.

WHAT SECTION DESCRIBES EXTENDED SOURCE PDFs

4.4 The LAT Instrument Response Functions

The performance of the LAT is composted of two effects. The efficiency of the LAT referes to its ability to to reconstruct a photon which comes into the detect. The disperson of the LAT refers to the probability of misreconstructing an event.

The efficiency is typically called the effective area. We write it as $\epsilon(E, t, \vec{\Omega})$. It is a function of energy, time, and solid angle (SA). It is measured in units of area (cm^2).

LINK TO arXiv:1206.1896 for MORE THOUROUGH DISCUSSION OF EFFECTIVE AREA

DISCUSS HOW EFFECTIVE AREA IS A FUNCTION OF DIFFERENT THINGS

The dispersion is the probability of a photon with true energy E and incoming direction $\vec{\Omega}$ at time t being reconstructed to to have an energy E', an incomming direction $\vec{\Omega}'$ at a time t'. The dispersion is written as $P(E', t', \vec{\Omega}'|E, t, \vec{\Omega})$. It represents a probability and is therefore normalized such that

$$\int\int\int \mathrm{d}E d\Omega \mathrm{d}t P(E', t', \vec{\Omega}'|E, t, \vec{\Omega}) = 1 \tag{4.9}$$

What is the range of the integrals

Therefore, $P(E', t', \vec{\Omega}'|E, t, \vec{\Omega})$ has units of 1/energy/SA/time

We assume these two factors to decouple and write the LAT's instrument response as

$$R(E', \vec{\Omega}', t'|E, \vec{\Omega}, t) = \epsilon(E, t, \vec{\Omega}) P(E', t', \vec{\Omega}'|E, t, \vec{\Omega}) \tag{4.10}$$

Therefore, the instrument response has units of area/energy/SA/time

The convolution of the flux of a model with the instrument response produces the expected counts per unit energy/time/SA begin reconstructed to have an energy E' at a position $\vec{\Omega}'$ and at a time t':

$$\tau(E', \vec{\Omega}', t'|\boldsymbol{\lambda}) = \int\int\int \mathrm{d}E\, d\Omega\, \mathrm{d}t\, \mathcal{F}(E, t, \vec{\Omega}|\boldsymbol{\lambda}) R(E', \vec{\Omega}', t'|E, \vec{\Omega}, t) \tag{4.11}$$

Here, this integral is performed over all true energies, SAs, and times for which the source model has support.

For LAT analysis, we conventionally make the simplifying assumption that the energy , spatial , and time dispersion decouple:

$$P(E', t', \vec{\Omega}'|E, t, \vec{\Omega}) = \mathrm{PSF}(\vec{\Omega}'|E, \vec{\Omega}) \times \mathrm{E_{disp}}(E'|E) \times \mathrm{T_{disp}}(t'|t) \tag{4.12}$$

Here, PSF is the point-spread function and represents ...

BETTER DISCUSSION OF PSF OF THE LAT, WHAT ITS SCALE IS...

$\mathrm{E_{disp}}$ represents the energy dispersion of the LAT. The energy dispersion of the LAT is a function of both the incident energy and incident angle of the photon. It varies from $\sim$ 5% to 20%, degrading at lower energies due to energy losses in the tracker and at higher energy due to electromagnetic shower losses outside the calorimiter. Similarly, it improves for photons with higher incident angles that are allowed a longer path through the calorimieter (Ackermann et al. 2012).

For sources with smoothly-varying spectra, the effects of ignoring the inherent energy dispersion of the LAT are typically small. Ackermann et al. (2012) performed a monte carlo simulation to show that for power-law point-like sources, the bias introduced by ignoring energy dispersion was on the level of a few perect. Therefore, energy dispersion is typicially ignored for standard likelihood analysis:

$$\mathrm{E_{disp}} = \delta(E - E') \tag{4.13}$$

We cauation that for analysis of sources extended to energies below 100 MeV and for sources expected to have spectra that do not smoothly vary, the effects of energy dispersion could be more severe.

- $\mathrm{T_{disp}}$ is the time dispersion.
-
- The timing dispersion is < 10 μs Atwood et al. (2009)
- WRITE ENERGY DISPERSION AS A DELTA FUNCTION

Why discard time dispersion

Therefore, the instrument response is typically approximated as FINISH

$$R(E', \vec{\Omega}', t'|E, \vec{\Omega},) = \epsilon(E, t', \vec{\Omega})\mathrm{PSF}(\vec{\Omega}'|E, \vec{\Omega}) \tag{4.14}$$

The expected count rate is then typically integrated over time to compute the total counts. Assuming that the source model is time indepdendent, we get:

$$\tau(E', \vec{\Omega}'|\boldsymbol{\lambda}) = \int d\Omega\, \mathcal{F}(E, \vec{\Omega}|\boldsymbol{\lambda}) \left(\int \mathrm{d}t\ \epsilon(E, t, \vec{\Omega}) \right) \mathrm{PSF}(\vec{\Omega}'|E, \vec{\Omega}) \tag{4.15}$$

This equation essentially says that the counts expected by the LAT for the particular model is the product of the source's flux with the effective area and then convolved with the point-spread function.

Figure out how the θ depedence of the IRFs factors into this calcualtion

4.5 Binned Maximum-Likelihood of LAT Data with the Science Tools

- For a standard LAT analysis, we perform a binned maximum-likelihood analysis:
- In the standard science tools, the data is binned in position and energy. and integrated in energy.
- For time-serires analysis, typically a time-summed analysyis is performed successivly in multiple time bins.
- The likelihood comes from a sum over each bin
- The likelihood is defined as

$$\mathcal{L} = \prod_j \frac{\theta_j^{n_j} e^{-\theta_j}}{n_j!} \tag{4.16}$$

  - Here, j is a sum over position/energy bins.

  - θ_j is the counts predicted by the model, which is defiend followign the discussion in Section 4.3.
  - n_j are the observed counts in the spatial/energy bin j

- The model counts are computed by integrating the differential counts defined in Equation 4.11 over the energy bin:

$$\theta_{ij} = \int_j \mathrm{d}E \; d\Omega \; \mathrm{d}t \; \tau(E, \vec{\Omega}, t|\boldsymbol{\lambda}_i) \tag{4.17}$$

  Here, j represents the integral over the jth position/energy bin, i represents the ith source, and $\boldsymbol{\lambda}_i$ refers to the parmeters defining the ith source. The total model counts is computed by summing over all sources:

$$\theta_j = \sum_i \theta_{ij} \tag{4.18}$$

- In the standard *Fermi* science tools, the binning of photons over position in the sky and energy to compute n_j is done with `gtbin`.
- In the standard *Fermi* science tools, the model counts θ_j are computed in several steps ...
- The instrument response is computed with a combination of `gtltcube`, `gtexpcube`.
- Convert a model of the sky into model predicted counts
- poisson likelihood
- Particular implemenation of maximum likelihood anlaysis
- Describe `gtbin`, `gtselect`, `gtlike`

Write Section or Perform simple MC Simulation to demonstrate signficance of detection

4.6 The Alternate Maximum-Likelihood Package `pointlike`

- Developed for Speed
- Sparce Matricies,
- Methods for computing integral model counts.

Chapter 5

Analysis of Spatially Extended LAT Sources

This chapter is based the first part of the the paper "Search for Spatially Extended Fermi-LAT Sources Using Two Years of Data" by Lande et at al. 2012 ApJ, 756, 5

5.1 Analysis Method

5.2 Validation of the TS Distribution

5.3 Extended Source Detection Threshold

5.4 Testing Against Source Confusion

5.5 Test of 2LAC Sources

5.6 Systematic Errors on Extension

Chapter 6

Search for Spatially-extended LAT Sources

This chapter is based the second part of the the paper "Search for Spatially Extended Fermi-LAT Sources Using Two Years of Data" by Lande et at al. 2012 ApJ, 756, 5

6.1 Extended Source Search Method

6.2 New Extended Sources

6.3 Discussion

Chapter 7

Search for Pulsar Wind Nebulae associated with Gamma-loud Pulsars

This chapter is basd on work from 2PC. GET REFERENCE HERE.

7.1 Off-peak Phase Selection

7.2 Off-peak Analysis Method

7.3 Off-peak Results

7.4 Off-Peak Individual Source Discussion

Chapter 8

Search for Pulsar Wind Nebulae associated with TeV Pulsars

Notes

- Only include sources classified as PWN in TeVCat.
- Always model LAT Pulsar in the background (???)

8.1 List of Candidates

8.2 Analysis Method

8.3 Sources Detected

Chapter 9

Search for Pulsar Wind Nebulae associated with High $\dot{E}$ Pulsars

Chapter 10

Population Study of The Large Area Telescope (LAT)-detected Pulsar wind nebula (PWN)

Chapter 11

Future Work (or Outlook)??

What would make good future work. Something about CTA population study, something about improved modeling liek HESS J1825, something about better PSF

Bibliography

Abdo, A. A., Ackermann, M., Ajello, M., et al. 2010a, ApJ, 708, 1254

—. 2010b, ApJS, 187, 460

Ackermann, M., Ajello, M., Albert, A., et al. 2012, ApJS, 203, 4

Aharonian, F., Akhperjanian, A. G., Bazer-Bachi, A. R., et al. 2006a, A&A, 460, 365

—. 2006b, ApJ, 636, 777

Aharonian, F. A., & Bogovalov, S. V. 2003, New A, 8, 85

Arnold, J. R., Metzger, A. E., Anderson, E. C., & van Dilla, M. A. 1962, J. Geophys. Res., 67, 4878

Arons, J. 1996, Space Sci. Rev., 75, 235

Ashworth, William B., J. 1981, Proceedings of the American Philosophical Society, 125, pp. 52

Atwood, W. B., Abdo, A. A., Ackermann, M., et al. 2009, ApJ, 697, 1071

Baum, W. A., Johnson, F. S., Oberly, J. J., et al. 1946, Phys. Rev., 70, 781

Bertsch, D. L., Brazier, K. T. S., Fichtel, C. E., et al. 1992, Nature, 357, 306

Bignami, G. F., Boella, G., Burger, J. J., et al. 1975, Space Science Instrumentation, 1, 245

Blandford, R. D., & Romani, R. W. 1988, MNRAS, 234, 57P

Bogovalov, S. V., & Aharonian, F. A. 2000, MNRAS, 313, 504

Bradt, H., Rappaport, S., & Mayer, W. 1969, Nature, 222, 728

Browning, R., Ramsden, D., & Wright, P. J. 1971, Nature Physical Science, 232, 99

Burnight, T. 1949, Phys. Rev, 76, 19

Caballero, I., & Wilms, J. 2012, Mem. Soc. Astron. Italiana, 83, 230

Carroll, B. W., & Ostlie, D. A. 2006, An Introduction to Modern Astrophysics, 2nd edn. (Benjamin Cummings)

Cash, W. 1979, ApJ, 228, 939

Chandrasekhar, S. 1931, ApJ, 74, 81

Cocke, W. J., Disney, M. J., & Taylor, D. J. 1969, Nature, 221, 525

Critchfield, C. L., Ney, E. P., & Oleksa, S. 1952, Physical Review, 85, 461

Demorest, P. B., Pennucci, T., Ransom, S. M., Roberts, M. S. E., & Hessels, J. W. T. 2010, Nature, 467, 1081

Espinoza, C. M., Lyne, A. G., Kramer, M., Manchester, R. N., & Kaspi, V. M. 2011, ApJ, 741, L13

Esposito, J. A., Bertsch, D. L., Chen, A. W., et al. 1999, ApJS, 123, 203

Falanga, M., Kuiper, L., Poutanen, J., et al. 2005, A&A, 444, 15

Feenberg, E., & Primakoff, H. 1948, Phys. Rev., 73, 449

Fichtel, C. E., Hartman, R. C., Kniffen, D. A., et al. 1975, ApJ, 198, 163

Fisher, R. A. 1925, Statistical Methods for Research Workers (Edinburgh: Oliver and Boyd)

Fritz, G., Henry, R. C., Meekins, J. F., Chubb, T. A., & Friedman, H. 1969, Science, 164, 709

Gaensler, B. M., & Slane, P. O. 2006, ARA&A, 44, 17

Gelfand, J. D., Slane, P. O., & Zhang, W. 2009, ApJ, 703, 2051

Gold, T. 1968, Nature, 218, 731

Goldreich, P., & Julian, W. H. 1969, ApJ, 157, 869

Grondin, M.-H., Funk, S., Lemoine-Goumard, M., et al. 2011, ApJ, 738, 42

Gunn, J. E., & Ostriker, J. P. 1969, Nature, 221, 454

Hartman, R. C., Bertsch, D. L., Bloom, S. D., et al. 1999, ApJS, 123, 79

Hayakawa, S. 1952, Progress of Theoretical Physics, 8, 571

Herschel, W. 1800, Philosophical Transactions of the Royal Society of London, 90, pp. 284

Hewish, A., Bell, S. J., Pilkington, J. D. H., Scott, P. F., & Collins, R. A. 1968, Nature, 217, 709

Hewitt, J., Grondin, M.-H., Lemoine-Goumard, M., et al. 2012

Hulsizer, R. I., & Rossi, B. 1948, Phys. Rev., 73, 1402

Hutchinson, G. 1952, Philosophical Magazine Series 7, 43, 847

Jansky, K. 1933, Proceedings of the Institute of Radio Engineers, 21, 1387

Kaspi, V. M., & Helfand, D. J. 2002, in Astronomical Society of the Pacific Conference Series, Vol. 271, Neutron Stars in Supernova Remnants, ed. P. O. Slane & B. M. Gaensler, 3

Katsuta, J., Uchiyama, Y., Tanaka, T., et al. 2012

Kennel, C. F., & Coroniti, F. V. 1984, ApJ, 283, 710

Kerr, M. 2010, PhD thesis, University of Washington

Kniffen, D. A., & Fichtel, C. E. 1970, ApJ, 161, L157

Kraushaar, W., Clark, G. W., Garmire, G., et al. 1965, ApJ, 141, 845

Kraushaar, W. L., Clark, G. W., Garmire, G. P., et al. 1972, ApJ, 177, 341

Large, M. I., Vaughan, A. E., & Mills, B. Y. 1968, Nature, 220, 340

Li, T.-P., & Ma, Y.-Q. 1983, ApJ, 272, 317

Mattox, J. R., Bertsch, D. L., Fichtel, C. E., et al. 1992, ApJ, 401, L23

Mattox, J. R., Bertsch, D. L., Chiang, J., et al. 1996, ApJ, 461, 396

Mayer-Hasselwander, H. A., Kanbach, G., Bennett, K., et al. 1982, A&A, 105, 164

McK Mahille, J., Schild, R., Wendorf, F., & Brenmer, R. 2007, African Skies, 11, 2

Morrison, P. 1958, Il Nuovo Cimento, 7, 858

Nolan, P. L., Arzoumanian, Z., Bertsch, D. L., et al. 1993, ApJ, 409, 697

Nolan, P. L., Fierro, J. M., Lin, Y. C., et al. 1996, A&AS, 120, C61

Nolan, P. L., Abdo, A. A., Ackermann, M., et al. 2012, ApJS, 199, 31

Pacini, F. 1967, Nature, 216, 567

—. 1968, Nature, 219, 145

Pacini, F., & Salvati, M. 1973, ApJ, 186, 249

Rea, N., & Esposito, P. 2011, in High-Energy Emission from Pulsars and their Systems, ed. D. F. Torres & N. Rea, 247

Rees, M. J., & Gunn, J. E. 1974, MNRAS, 167, 1

Richards, D. W., & Comella, J. M. 1969, Nature, 222, 551

Rousseau, R., Grondin, M.-H., Van Etten, A., et al. 2012, A&A, 544, A3

Slane, P., Castro, D., Funk, S., et al. 2010, The Astrophysical Journal, 720, 266

Sreekumar, P., Bertsch, D. L., Hartman, R. C., Nolan, P. L., & Thompson, D. J. 1999, Astroparticle Physics, 11, 221

Sreekumar, P., Bertsch, D. L., Dingus, B. L., et al. 1992, ApJ, 400, L67

Staelin, D. H., & Reifenstein, III, E. C. 1968, Science, 162, 1481

Swanenburg, B. N., Hermsen, W., Bennett, K., et al. 1978, Nature, 275, 298

Swanenburg, B. N., Bennett, K., Bignami, G. F., et al. 1981, ApJ, 243, L69

Thompson, D. J. 2008, Reports on Progress in Physics, 71, 116901

Thompson, D. J., Fichtel, C. E., Hartman, R. C., Kniffen, D. A., & Lamb, R. C. 1977a, ApJ, 213, 252

Thompson, D. J., Fichtel, C. E., Kniffen, D. A., & Ogelman, H. B. 1977b, ApJ, 214, L17

Thompson, D. J., Bertsch, D. L., Fichtel, C. E., et al. 1993, ApJS, 86, 629

van der Swaluw, E., & Wu, Y. 2001, ApJ, 555, L49